Journal of Advanced Ceramics
2016, **5**(1): 47–53
DOI: 10.1007/s40145-015-0172-y

ISSN 2226-4108
CN 10-1154/TQ

Research Article

Bioactivity of quaternary glass prepared from bentonite clay

Luqman A. ADAMS[a,*], Enobong R. ESSIEN[b]

[a]*Department of Chemistry*, *University of Lagos*, *Nigeria*
[b]*Department of Chemical Sciences*, *Bells University of Technology*, *P.M.B 1015 Ota*, *Ogun*, *Nigeria*

Received: July 27, 2015; Revised: September 15, 2015; Accepted: October 14, 2015

Abstract: Alkoxysilane precursors are the most widely used silica source for sol–gel preparation of silicate-based bioactive glass. However, due to their high cost, alternative sources such as bentonite clay are desirable. In the present work, bentonite clay was reacted with sodium hydroxide (NaOH) to extract sodium metasilicate (Na_2SiO_3). The obtained Na_2SiO_3 was converted to gel which was then sintered at 950 ℃ for 3 h to give the bioactive glass in the quaternary composition SiO_2–NaO–CaO–P_2O_5. The resulting glass was incubated in simulated body fluid (SBF) for 0–7 days to evaluate the bioactivity. Furthermore, glass samples were characterized before and after SBF study by scanning electron microscopy (SEM), energy dispersive X-ray spectroscopy (EDX), X-ray diffraction (XRD), and Fourier transform infrared spectroscopy (FTIR). Results obtained showed the presence of $Na_2Ca_2Si_3O_9$ (combeite) crystal as the major crystalline phase and the formation of hydroxyapatite (HA) and hydroxycarbonated apatite (HCA) on the surface of the glass after immersion in SBF. The material showed potentials for application as scaffold in bone tissue repair.

Keywords: bentonite clay; bioactivity; alkoxysilane; hydroxyapatite (HA); bone repair

1 Introduction

The interest in bioactive glass has continued to soar particularly within the orthopaedic biomedical research community because of its ability to promote self-repair of damaged bones when used as temporary scaffold *in vivo*. The "gold standard" for bone treatment involves autograft and allograft transplantation. However, these methods have severe limitations and thus impose high cost on the health care system. The shortcomings associated with autograft include severe pain, morbidity of the harvested site, structural and anatomical problems, and high rate of resorption during healing [1,2]. Likewise, allograft may elicit disease transmission and rejection, further compounded by shortage of donors [3,4].

The use of bioactive glass for bone restoration represents a paradigm shift from replacement to regeneration through the use of synthetic bone grafts as positive effort to address the aforementioned drawbacks. The unique capability of bioactive glass over other bioceramics includes amongst others the ability to form hydroxyapatite (HA) on the surface when immersed in physiological environment [5,6]. This is beneficial because of the similarity in chemical composition of HA to bone and therefore facilitates the bonding between the material and bone [7]. Other significance of bioactive glass in physiological environment is its ability to elicit osteoblastic activity and improvement of cell adhesion [8]. Indeed, it has been reported that seven families of genes are up-regulated by the ionic dissolution products from

* Corresponding author.
E-mail: ladams@unilag.edu.ng

bioactive glass [9].

Generally, sol–gel-derived glass, with its inherent mesoporosity, provides larger surface area and consequently more rapid degradation rate than melt-derived glass of similar composition [10,11]. Additionally, the sol–gel technology provides higher purity, homogeneity, and possibility of increasing the compositional range above 60 mol% while maintaining bioactivity of the glass [12].

Recently, our research group embarked on the search for new silica-based materials as economic synthetic substitutes to the widely used alkoxysilane precursors such as tetraethyl orthosilicate (TEOS) and tetramethyl othosilicate (TMOS). Consequently, we have reported the synthesis of bioactive glass from sand and clay using the sol–gel technique [13,14]. However, in our use of bentonite clay as a novel starting material [14], we did not evaluate the bioactivity of the obtained bioceramic, and to the best of our knowledge, no previous work on the bioactivity of sol–gel-derived bioactive glass from bentonite clay has yet been reported. Therefore, herein we report the bioactivity of quaternary bioactive glass in the system SiO_2–Na_2O–CaO–P_2O_5 obtained from bentonite clay.

2 Materials and methods

2. 1 Materials

The chemicals for the preparation of the bioactive glass included: bentonite clay -$(OH)_4Si_8Al_4O_{20}\cdot nH_2O$ (Ijero-Ekiti, Nigeria), sodium hydroxide (Sigma-Aldrich, 99%), nitric acid (HNO_3, Fluka, Germany), phosphoric acid (H_3PO_4, BDH Laboratory, 98%), sodium nitrate ($NaNO_3$, Sigma-Aldrich, 99%), and calcium nitrate tetrahydrate ($Ca(NO_3)_2\cdot 4H_2O$, LOBA, 98%). All chemicals were used as obtained without further purification.

2. 2 Methods

To prepare the bioactive glass with composition 46.99 mol% SiO_2, 24.36 mol% Na_2O, 25.50 mol% CaO, and 3.15 mol% P_2O_5, sodium metasilicate (Na_2SiO_3) was first extracted from bentonite clay as described previously [15]. In a typical sol–gel procedure, appropriate amount of the obtained Na_2SiO_3 was dissolved in deionized water to give a solution that was then added slowly to 1 M HNO_3 in a beaker furnished with a magnetic stirrer under ambient temperature for 1 h to facilitate complete hydrolysis. Thereafter, H_3PO_4, $NaNO_3$, and $Ca(NO_3)_2\cdot 4H_2O$ were added under constant stirring to give a molar ratio 1:10 of each reagent to water in the sol. A reaction time of 45 min was allowed for each reagent before adding the next. After complete addition, the mixture was further stirred for 1 h to afford a gel. The resulting gel was aged at room temperature for 3 days, dried at 60 ℃ for 72 h and 130 ℃ for 42 h, and stabilized at 700 ℃ for 2 h. Finally, the material was sintered at 950 ℃ for 3 h for densification and strengthening of pore struts.

2. 3 Characterization

The density of the bioactive glass ρ_{glass} was calculated from the mass and dimensions of the sintered glass. The porosity P was then obtained mathematically as follows:

$$P = \left(1 - \frac{\rho_{glass}}{\rho_s}\right) \times 100 \quad (1)$$

where $\rho_s = 2.7$ g/cm^3 is the theoretical density of 45S5 Bioglass® [16].

The microstructure, composition, and pore size distribution of the glass were evaluated in a Phenom Prox (Eindhoven, the Netherlands) scanning electron microscope (SEM) equiped with energy dispersive X-ray analyzer (EDX) before and after immersion in simulated body fluid (SBF). The sample was carbon-coated and observed at an accelerating voltage of 15 kV.

Samples were characterized using X-ray diffraction (XRD) analysis after sintering and after each immersion experiment in SBF with the aim of assessing the major phase present and the formation of hydroxyapatite (HA) crystal on samples' strut surface respectively. The samples were first ground to powder. Then 0.1 g of the powder was measured in a PANalytical Empyrean X-ray diffractometer using Cu Kα radiation source of wavelength $\lambda = 0.154056$ nm operated at 40 kV and 40 mA to obtain the diffraction patterns in the 2θ range from 5° to 90°.

Fourier transform infrared spectroscopy (FTIR, Shimadzu 8400S), with wavenumber range of 4000–400 cm^{-1} employing KBr pellets and operating in a reflectance mode with 4 cm^{-1} resolution, was employed to monitor the nature of bonds present in the as prepared samples.

2. 4 *In vitro* bioactivity assessment in simulated body fluid

Evaluation of bone bonding ability was carried out by the standard *in vitro* procedure [17]. The acellular simulated body fluid (SBF) was prepared using analytical reagent-grade chemicals NaCl, $NaHCO_3$, KCl, $K_2HPO_4{\cdot}3H_2O$, $MgCl_2{\cdot}6H_2O$, $CaCl_2$, trishydroxymethyl aminomethane (Tris-buffer, $(CH_2OH)_3CNH_2$), and 1 M HCl with ion concentrations shown in Table 1. Samples were immersed in the SBF solution at a concentration of 0.01 g/mL in clean plastic bottles, which were initially washed using HCl and deionized water. The bottles were placed inside a thermostated incubator at a temperature of 36.5 ℃ and an initial pH of 7.4. The SBF solutions were not refreshed throughout the period of immersion to allow for measurement of pH of the solution at different intervals between 0 and 120 h duration using a pH meter (Hanna, HI96107) previously calibrated with buffer solutions of pH = 4.0, 7.0, and 9.0. The samples were extracted from the SBF solution after 3 and 7 days. The extracted samples were rinsed with deionized water and left to dry at ambient temperature in a desiccator. The formation of apatite layer on the glass surface was monitored by SEM, EDX, XRD, and FTIR.

3 Results

3. 1 Changes in morphology

The morphology of the glass before and after immersion in SBF is shown in Fig. 1. As observed in Fig. 1(a), before immersion, the glass presents almost uniform porous surface containing mostly cuboid-shaped glass architecture well distributed throughout the material. The porosity of the glass obtained by applying Eq. (1) is 82%. After immersion in SBF for 3 days, the glass morphology changes to fine grain-sized particles, most of which are agglomerated as shown in Fig. 1(b). The EDX spectrum during this period of immersion shows a decrease in the concentrations of Na, Si, and Ca but an increase in P. These changes can be attributed to the formation of HA on the surface of the glass. After immersion for 7 days in SBF (Fig. 1(c)), the micrograph shows dense clusters of HA particles, which also appear coarse. Accordingly, the EDX spectrum records low detection of Si due to increase in population of apatite on the glass surface, while the concentrations of Ca and P increase. Furthermore, a small carbon peak becomes evident indicating the formation of crystalline hydroxycarbonated apatite (HCA).

Table 1 Ion concentration in human plasma in comparison with SBF (unit: mM)

Ion	Na^+	K^+	Mg^{2+}	Ca^{2+}	Cl^-	HCO_3^-	HPO_4^{2-}	SO_4^{2-}
SBF	142.0	5.0	1.5	2.5	147.8	4.2	1.0	0.5
Human plasma	142.0	5.0	1.5	2.5	103.0	27.0	1.0	0.5

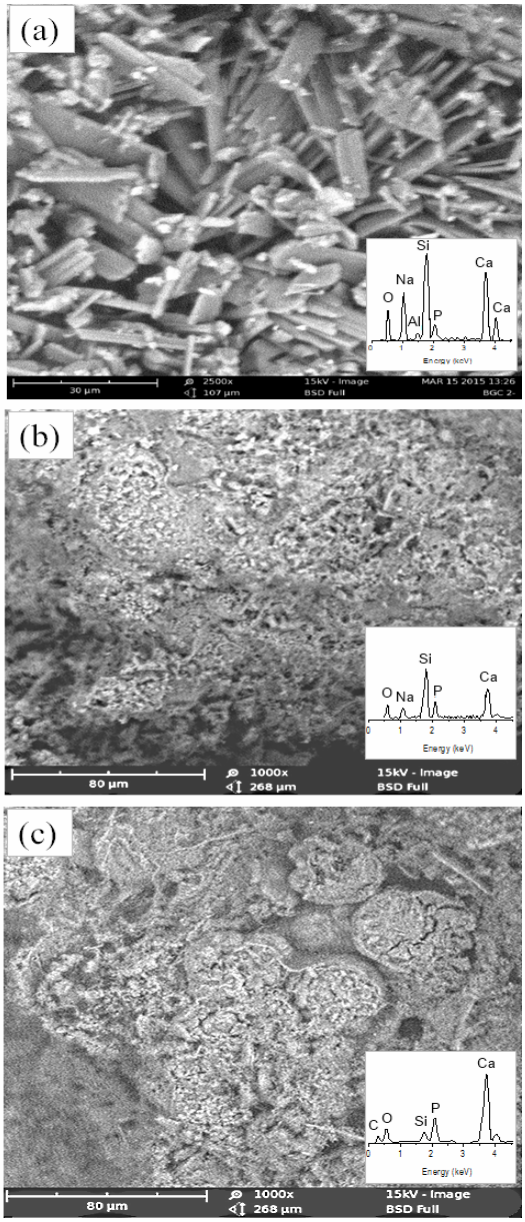

Fig. 1 SEM micrographs with EDX insets of the bioactive glass showing the growth of apatite: (a) as sintered, (b) after soaking in SBF for 3 days, and (c) after soaking in SBF for 7 days.

3. 2 Diffraction patterns

The XRD investigation of the glass samples after annealing at 950 ℃ for 3 h reveals the presence of major peaks of combeite ($Na_2Ca_2Si_3O_9$) crystal usually formed from devitrification of quaternary system of SiO_2–Na_2O–CaO–P_2O_5 bioactive glass [18,19] as shown in Fig. 2(a). Both the angular location and intensity of the peaks match the standard PDF #22.1455. As seen, it is obvious that the glass does not fully crystallize judging by the low intensities of the $Na_2Ca_2Si_3O_9$ peaks at locations other than the one at $2\theta \approx 30°$. Even before immersion in SBF, a peak identified as apatite is clearly visible at $2\theta \approx 32°$. This phenomenon has been attributed to the aqueous environment of the sol–gel process which favours the precipitation of HA from the amorphous structure of silica-based bioactive glass [20].

After immersion in SBF, the intensity of the $Na_2Ca_2Si_3O_9$ peaks decreases gradually as shown in Figs. 2(a)–2(c). The gradual decrease is an indication that the material could have controlled degradation rate in physiological fluids, and hence is able to act as temporary scaffold prior to complete integration of the damaged site, as a major requirement of an ideal scaffold for bone repair [21]. Apatite peaks increase as immersion duration is prolonged. All apatite positions are corroborated by those in the standard PDF JCPDS #9-0432.

3. 3 Assessment of bonds

The FTIR spectrum of the pristine bioactive glass is shown in Fig. 3(a). As observed, there are prominent peaks at 3462, 1684, 1458, 1005, 850, 602, and 457 cm^{-1}. The broad band between 3300 and 3800 cm^{-1} centred at 3462 cm^{-1} is due to OH groups in the material, which is further confirmed by the presence of water absorbed band around 1684 cm^{-1}. The band at 1458 cm^{-1} is representative of the absorption of carbonate group (ν_3), while the sharp peak at 1005 cm^{-1} is associated with Si–O–Si vibrational modes [22]. The peak at 850 cm^{-1} is synonymous with C–O stretching vibration [22], which may be due to adsorption of atmospheric CO_2 during the processing stage of the glass. There is an intense peak at 602 cm^{-1} which is assigned to P–O bending mode in crystalline calcium phosphate, and another small peak at 457 cm^{-1} is attributed to Si–O–Si bending vibrations. After immersion for 3 days (Fig. 3(b)), the peak at 1458 cm^{-1} becomes broader and splits into two modes at 1476 and 1424 cm^{-1}, and similarly the peak at 602 cm^{-1} develops into two modes at 604 and 569 cm^{-1}. These are characteristics of apatite crystalline phase [23], signalling the incorporation of CO_3^{2-} from the SBF solution into HA on the glass surface to form HCA. While after 7-day immersion in SBF (Fig. 3(c)), the twin peaks at 604 and 569 cm^{-1} become more intense due to increase in density of HCA on the surface of the glass, thus explaining the appearance of the small carbon peak observed in the EDX spectrum (Fig. 1(c) inset).

3. 4 Reactivity in SBF

Figure 4 shows the pH change of the glass in SBF for the first 120 h, which is in agreement with the reaction sequence of bioactive glass in biological fluids [5]. As observed, there is fast release of alkali and alkaline

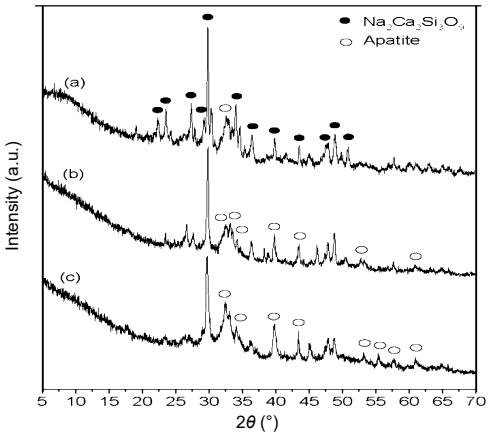

Fig. 2 XRD spectra of the bioactive glass during the period of incubation for (a) 0 day, (b) 3 days, and (c) 7 days showing phases present.

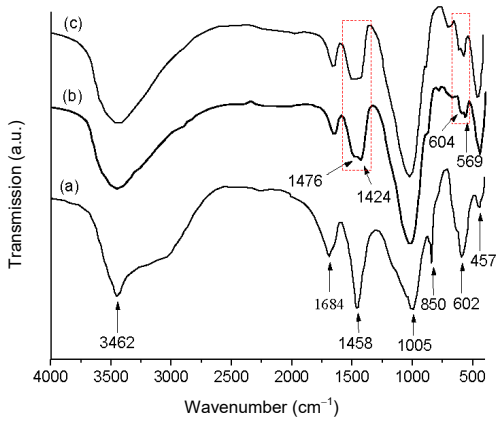

Fig. 3 FTIR spectra of the glass immersed in SBF for (a) 0 day, (b) 3 days, and (c) 7 days. Similar absorption patterns are marked in red doted rectangle.

earth ions (Na^+ and Ca^{2+}) from the glass into SBF solution during the first 4 h leading to an increase in pH of the solution from the initial 7.4 to 10.0. The first stage of the reaction involves ion-exchange between Na^+ and Ca^{2+} of the glass with H^+ or H_3O^+ of the solution [18]:

$$\equiv Si{-}O^{-}Na^{+} + H^{+} \longrightarrow \equiv Si{-}OH + Na^{+}(aq) \quad (2)$$

After 4 h, the pH increases slowly until 48 h because part of the released Ca^{2+} from the glass is used to form $CaO–P_2O_5$, thus decreasing the release rate as shown in Fig. 4. As immersion duration reaches 96 h, the pH increase slows further as more Ca^{2+} is withdrawn from the SBF solution to develop HCA layer on the surface of the glass. Finally, the pH reaches a saturated value of 11.7 after 96 h without increasing any further due to crystallization of HCA.

4 Discussion

4. 1 Composition

Bentonite clay, a naturally occurring sedimentary clay with the chemical formula $(OH)_4Si_8Al_4O_{20}\cdot nH_2O$, has a 3-layer structure displaying one aluminium oxide sheet sandwiched by two silicon oxide sheets. The arrangement is such that Mg^{2+} ions may substitute for Al^{3+} ions leaving a net negative charge on the sheets [14]. The clay is reacted with NaOH to extract the Si^{4+} ions from the sheets to form Na_2SiO_3 as filtrate and $Al(OH)_3$ as residue as shown in a previous reaction scheme [14]. The obtained Na_2SiO_3 then serves as precursor for SiO_2 and Na_2O for preparing the glass. The EDX result of the sintered glass as shown in Fig. 5 confirms the presence of all the elements in their appropriate ratios as prepared. Additionally, a residual

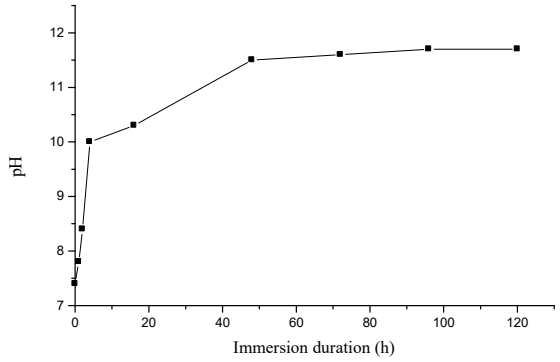

Fig. 4 pH change of the glass during immersion in SBF for 120 h.

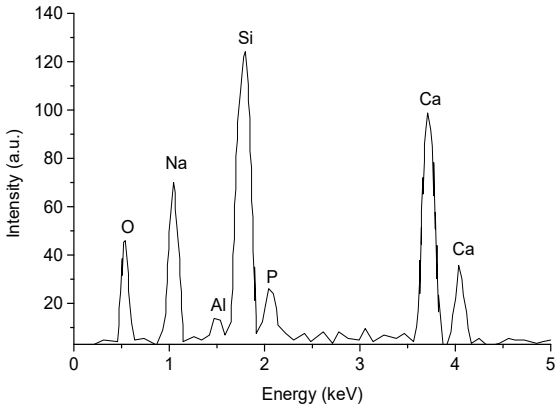

Fig. 5 Elemental composition of the parent glass as measured by EDX.

peak of Al observed in the spectrum may be due to incomplete removal of $Al(OH)_3$ from the Na_2SiO_3 filtrate during the extraction stage. Hence a more efficient filtration method, such as vacuum filtration, may be necessary. Apart from bentonite clay, kaolinite clay ($Al_2Si_2O_5(OH)_4$) could serve as another cheap alternative source of silica.

4. 2 Microstructure

The glass exhibits sub-micron pore diameter of mean value 2.54 μm (Fig. 6(a)), while the average pore area is 0.29 μm^2 (Fig. 6(b)). This is expected as clay particles themselves have dimensions on nanoscale [24,25], thus arrangement of these particles leads to evolution of large surface area associated with sub-micron pore structure as observed in Fig. 6. The microstructure of the glass as well as its porosity of 82% are crucial textural parameters for enhanced cell adhesion, vascularisation, infiltration, and osteointegration on the glass material [26–31].

4. 3 $Na_2Ca_2Si_3O_9$ crystalline phase

The $Na_2Ca_2Si_3O_9$ crystal detected in the XRD spectrum (Fig. 2) is the major crystalline phase, and displays cuboidal architecture as seen in the SEM micrograph shown in Fig. 1(a). During sintering, Na_2O, CaO, and SiO_2 present in the composition react to form $Na_2Ca_2Si_3O_9$. Mechanical strength is a significant factor in the choice of an ideal scaffold to serve as temporary support for new bone growth [31]. While there have been concerns about the biodegradability of crystalline $Na_2Ca_2Si_3O_9$, some authors have reported different scaffold designs and synthetic route optimization to improve degradation behaviour of $Na_2Ca_2Si_3O_9$ in physiological fluids [31–33]. In the

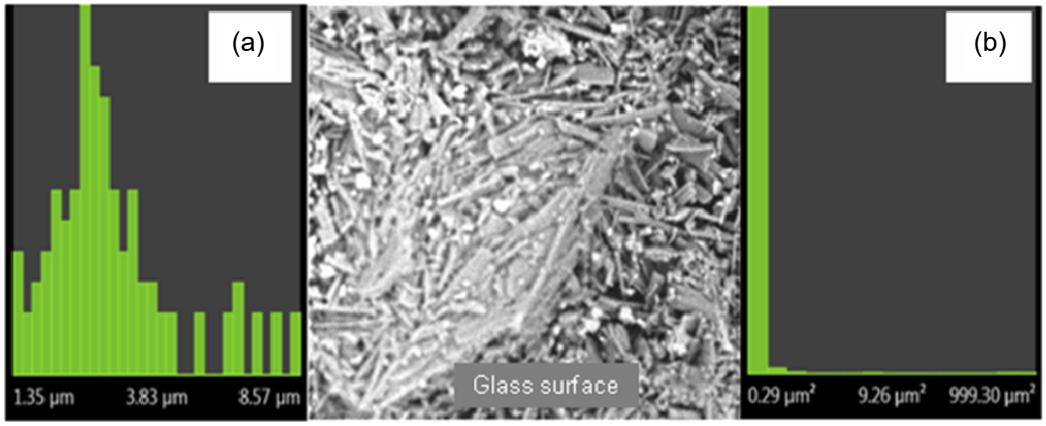

Fig. 6 Fibrematrics of the glass after sintering showing (a) pore size distribution and (b) average pore area of the glass surface (middle) as determined by SEM.

present work, to ensure partial crystallization, the sintering protocol was set at 950 ℃ for 3 h. The gradual transformation of the glass from crystalline to amorphous after soaking in SBF for 7 days indicates biodegradability [26,34–38].

4. 4 pH change in SBF

The steep rise in pH during the first 4 h of soaking in SBF indicates high reactivity of the glass. The large surface area conferred on the glass by well distributed particles and sub-micron-sized pores presents optimal sites for ion-exchange reaction to occur. This phenomenon explains why apatite nucleation occurs at a shorter time, even without immersion in SBF, as observed in the spectra for XRD and FTIR in Fig. 2(a) and Fig. 3(a) respectively. At the end of 120 h (5 days), the pH reaches a value of 11.7 from the initial 7.4 during which apatite colony increases on the surface of the glass as evident by the low detection of Si recorded by EDX shown in Fig. 1(a). The basis of bonding property of bioactive glass has been anchored on the chemical reactivity in physiological body fluids (*in vitro* and *in vivo*), which leads to the formation of HCA layer to which bone can bond.

5 Conclusions

The highly bioactive glass in quaternary composition has been prepared starting with bentonite clay as silica source instead of conventional alkoxysilane precursors. The large surface area and micron-sized pore structure obtained through the sol–gel processing method were key in accelerating the reactivity of the glass in SBF to form apatite. The crystalline $Na_2Ca_2Si_3O_9$ formed from sintering the glass is important in reinforcing the strength of the material during application as scaffold in bone repair. Interestingly, the crystalline phase did not hinder the biodegradability of the glass in SBF. With continuing efforts geared towards cost effective design of scaffolds for optimal bioactivity, bentonite clay may be a potential cheap raw material for the preparation of bioactive glass.

Acknowledgements

The authors are thankful to Mr. Femi Igbari of the College of NanoScience and Technology, Soochow University, China, for his assistance with the EDX and XRD characterisations as well as Mr. Isa Yakubu of Ahmadu Bello University Zaria for the SEM analysis.

References

[1] Lee S-C, Chen J-F, Wu C-T, *et al*. *In situ* local autograft for instrumented lower lumbar or lumbosacral posterolateral fusion. *J Clin Neurosci* 2009, **16**: 37–43.

[2] Damien CJ, Parsons JP. Bone graft and bone substitutes: A review of current technology and applications. *J Appl Biomater* 1991, **2**: 187–208.

[3] Calori GM, Mazza E, Colombo M, *et al*. The use of bone-graft substitutes in large bone defects: Any specific needs? *Injury* 2011, **42**: S56–S63.

[4] Rose FRAJ, Oreffo ROC. Bone tissue engineering: Hope vs hype. *Biochem Bioph Res Co* 2002, **292**: 1–7.

[5] Hench LL. Bioceramics. *J Am Ceram Soc* 1998, **81**: 1705–1728.

[6] Rahaman MN, Day DE, Bal BS, *et al*. Bioactive glass in tissue engineering. *Acta Biomater* 2011, **7**: 2355–2373.

[7] Oonishi H, Hench LL, Wilson J, *et al.* Comparative bone growth behaviour in granules of bioceramic materials of

various sizes. *J Biomed Mater Res* 1999, **44**: 31–43.
[8] Olmo N, Martin AI, Salinas AJ, *et al*. Bioactive sol–gel glasses with and without a hydroxycarbonate apatite layer as substrates for osteoblast cell adhesion and proliferation. *Biomaterials* 2003, **24**: 3383–3393.
[9] Jell G, Stevens MM. Gene activation by bioactive glasses. *J Mater Sci: Mater M* 2006, **17**: 997–1002.
[10] Pereira MM, Jones JR, Orefice RL, *et al*. Preparation of bioactive glass-polyvinyl alcohol hybrid foams by the sol–gel method. *J Mater Sci: Mater M* 2005, **16**: 1045–1050.
[11] Wu C, Luo Y, Cuniberti G, *et al*. Three-dimensional printing of hierarchical and tough mesoporous bioactive glass scaffolds with a controllable pore architecture, excellent mechanical strength and mineralization ability. *Acta Biomater* 2011, **7**: 2644–2650.
[12] Fardad MA. Catalysis and structure of SiO_2 sol–gel films. *J Mater Sci* 2000, **35**: 1835–1841.
[13] Essien ER, Adams LA, Shaibu, RO, *et al*. Economic route to sodium-containing silicate bioactive glass scaffold. *Open Journal of Regenerative Medicine* 2012, **1**: 33–40.
[14] Essien ER, Adams LA, Shaibu, RO, *et al*. Sol–gel bioceramic material from bentonite clay. *Journal of Biomedical Science and Engineering* 2013, **6**: 258–264.
[15] Essien ER, Olaniyi OA, Adams LA, *et al*. Sol–gel-derived porous silica: Economic synthesis and characterization. *Journal of Minerals and Materials Characterization and Engineering* 2012, **11**: 976–981.
[16] Cao W, Hench LL. Bioactive materials. *Ceram Int* 1996, **22**: 493–507.
[17] Kokubo T, Takadama H. How useful is SBF in predicting *in vivo* bone bioactivity? *Biomaterials* 2006, **27**: 2907–2915.
[18] Clupper DC, Mecholsky Jr. JJ, LaTorre GP, *et al*. Sintering temperature effects on the *in vitro* bioactive response of tape cast and sintered bioactive glass-ceramic in Tris buffer. *J Biomed Mater Res* 2001, **57**: 532–540.
[19] Clupper DC, Mecholsky Jr. JJ, LaTorre GP, *et al*. Bioactivity of tape cast and sintered bioactive glass-ceramic in simulated body fluid. *Biomaterial*s 2002, **23**: 2599–2606.
[20] Chen Q-Z, Li Y, Jin L-Y, *et al.* A new sol–gel process for producing Na_2O-containing bioactive glass ceramics. *Acta Biomater* 2010, **6**: 4143–4153.
[21] Gerhardt L-C, Boccaccini AR. Bioactive glass and glass-ceramic scaffolds for bone tissue engineering. *Materials* 2010, **3**: 3867–3910.
[22] Peitl O, Zanotto ED, Hench LL. Highly bioactive P_2O_5–Na_2O–CaO–SiO_2 glass-ceramics. *J Non-Cryst Solids* 2001, **292**: 115–126.
[23] Oliveira JM, Correia RN, Fernandes MH. Effects of Si speciation on the *in vitro* bioactivity of glasses. *Biomaterials* 2002, **23**: 371–379.
[24] Alexandre M, Dubois P. Polymer-layered silicate nanocomposites: Preparation, properties and uses of a new class of materials. *Mat Sci Eng R* 2000, **28**: 1–63.
[25] Katti KS, Katti DR. Relatioship of swelling and swelling pressure on silica–water interactions in montmorillonite. *Langmuir* 2006, **22**: 532–537.
[26] Rezwan K, Chen QZ, Blaker JJ, *et al*. Biodegradable and bioactive porous polymer/inorganic composite scaffolds for bone tissue engineering. *Biomaterials* 2006, **27**: 3413–3431.
[27] Vitale-Brovarone C, Miola M, Balagna C, *et al*. 3D-glass-ceramic scaffolds with antibacterial properties for bone grafting. *Chem Eng J* 2008, **137**: 129–136.
[28] Karageorgiou V, Kaplan D. Porosity of 3D biomaterial scaffolds and osteogenesis. *Biomaterials* 2005, **26**: 5474–5491.
[29] Smith IO, Ren F, Baumann MJ, *et al*. Confocal laser scanning microscopy as a tool for imaging cancellous bone. *J Biomed Mater Res B* 2006, **79**: 185–192.
[30] Woodard JR, Hilldore AJ, Lan SK, *et al*. The mechanical properties and osteoconductivity of hydroxyapatite bone scaffolds with multi-scale porosity. *Biomaterials* 2007, **28**: 45–54.
[31] Vitale-Brovarone C, Baino F, Verné E. High strength bioactive glass-ceramic scaffolds for bone regeneration. *J Mater Sci: Mater M* 2009, **20**: 643–653.
[32] Du R, Chang J. Preparation and characterization of bioactive sol–gel-derived $Na_2Ca_2Si_3O_9$. *J Mater Sci: Mater M* 2004, **15**: 1285–1289.
[33] Filho OP, LaTorre GP, Hench LL. Effect of crystallization on apatite-layer formation of bioactive glass 45S5. *J Biomed Mater Res* 1996, **30**: 509–514.
[34] Chen QZ, Thompson ID, Boccaccini AR. 45S5 Bioglass®-derived glass-ceramic scaffolds for bone tissue engineering. *Biomaterials* 2006, **27**: 2414–2425.
[35] Hench LL, Polak JM. Third-generation biomedical materials. *Science* 2002, **295**: 1014–1017.
[36] Hench LL. The story of Bioglass®. *J Mater Sci: Mater M* 2006, **17**: 967–978.
[37] Hench LL Bioceramics: From concept to clinic. *J Am Ceram Soc* 1991, **74**: 1487–1510.
[38] Hench LL, Andersson Ö. Bioactive glasses. In: *An Introduction to Bioceramics*. Hench LL, Wilson J, Eds. Singapore: World Scientific Publishing, 1993: 41–62.